Effect of processing parameters and clay volume fraction on the mechanical properties of epoxy-clay nanocomposites

S.C. ZUNJARRAO
Mechanics of Advanced Materials Laboratory, Department of Mechanical Engineering, State University of New York at Stony Brook, Stony Brook, NY, 11794-2300, USA

R. SRIRAMAN
John F Welch Technology Center, GE India Technology Center Pvt. Ltd., Bangalore 560 066, India

R.P. SINGH*
Mechanics of Advanced Materials Laboratory, Department of Mechanical Engineering, State University of New York at Stony Brook, Stony Brook, NY, 11794-2300, USA
E-mail: raman.singh@sunysb.edu

Published online: 3 March 2006

The influence of processing parameters and particle volume fraction was experimentally studied for epoxy clay nanocomposites. Nanocomposites were prepared using onium ion surface modified montmorillonite (MMT) layered clay and epoxy resin (DEGBF). Two different techniques were used for dispersing the clay particles in the epoxy matrix, viz. high-speed shear dispersion and ultrasonic disruption. The volume fraction of clay particles was systematically varied from 0.5 to 6%, and mechanical properties, viz. flexural modulus and fracture toughness, were studied as a function of clay volume fraction and the processing technique. The flexural modulus was observed to increase monotonously with increase in volume fraction of clay particles, while, the fracture toughness showed an initial increase on addition of clay particles, but a subsequent decrease at higher clay volume fractions. In general, nanocomposites processed by shear mixing exhibited better mechanical properties as compared to those processed by ultrasonication. Investigation by X-ray diffraction (XRD) revealed exfoliated clay structure in most of the nanocomposites that were fabricated. Morphologies of the fracture surfaces of nanocomposites were studied using a scanning electron microscopy (SEM). Presence of river markings at low clay volume fractions provided evidence of extrinsic toughening taking place in an otherwise brittle epoxy.

1. Introduction

It is common to reinforce polymers with a second organic or inorganic phase to produce a polymer composite. Polymer nanocomposites, where the size of the reinforcement phase is of the order of a few nanometers, offer an excellent alternative to neat polymers and conventional composites. In nano-scale particle reinforced polymer composites, the enhancement in mechanical properties is directly related to the surface area of the reinforcement [1]. For a given volume fraction, the surface area of these nano-scale fillers is much higher as compared to that of micron sized fillers. As a result, significant enhancement in various properties can be observed using very low volume fractions of nano-scale fillers. Since high degrees of stiffness and strength are realized with far less high-density inorganic material, polymer nanocomposites tend to be much lighter than conventional polymer composites that have typical filler volume fractions of 30–60%.

In recent years, researchers have developed and investigated polymer nanocomposites based on a wide variety of nano-scale fillers including clay particles (layered silicates) [2, 3], aluminum particles [4, 5], TiO_2 particles [6], carbon nanotubes [7], etc. Amongst various fillers, those based on layered silicates offer the greatest

*Author to whom all correspondence should be addressed.
0022-2461
DOI: 10.1007/s10853-006-7179-2

commercial potential because these clays are readily available, are cheaper than other nano-scale fillers and have well understood intercalation chemistry [1, 8, 9]. Because of the nanometer size particles obtained by dispersion of the individual clay platelets, polymer-clay nanocomposites have markedly improved mechanical, thermal and physico-chemical properties as demonstrated first by Toyota researchers in the early 1990s [10, 11]. The primary focus of these early investigations was to enhance the thermogravimetric properties and the modulus of thermoplastics such as nylon. It was reported that addition of as little as 2% volume of inorganic layered silicate with nylon-6 increased the tensile strength by 40% and modulus by 68%. The heat distortion temperature of nylon-clay composite was higher by 87°C as compared to neat nylon-6, which has a heat distortion temperature of 65°C. Motivated by these studies, many researchers have synthesized and studied the properties of various clay filled thermoplastic resins such as polyamides [12–14], polyimides [14–16], polyethylene [17, 18], poly(methyl methacrylate) [19, 20], ethylene vinyl acetate copolymers [21, 22] and so on. Alexandre and Dubois [23] provide a summary of different polymers and fabrication routes available in the literature. Recently, researchers have also focused on polymer-clay nanocomposites based on thermosetting resins, especially epoxy [9, 24, 25]. The focus of the current investigation is to study the effect of different processing techniques on the fracture toughness and flexural modulus of epoxy-clay nanocomposites.

Depending on the nature of components (clay and polymer), the method of preparation (melt, solution or in-situ polymerization) and the processing techniques used, various clay-polymer morphologies viz. phase separated, intercalated or exfoliated structure can be obtained [23]. It is generally believed that the improvement in properties of the clay nanocomposites is directly related to the complete exfoliation of silicate layers in the polymer. In epoxy based systems, the final structure of the clay particles depends on the type of resin and curing agent used and the rate of curing. For the case of highly flexible and low glass transition temperature epoxies, the addition of clay leads to a greater increase in the modulus and strength as compared to epoxies that are rigid and have a high glass transition temperature [26]. It has also been shown that difunctional epoxy systems and aliphatic diamine based curing agents favor exfoliation under optimum curing cycle [24, 27]. Polymerization is believed to be the indirect driving force for the exfoliation [28]. The clay, due to its high surface energy, attracts polar monomer molecules in the clay galleries until equilibrium is reached. The polymerization reactions occurring in the clay galleries lower the polarity of the intercalated molecules and displace the equilibrium. This allows new polar species to diffuse between the layers and progressively exfoliate the clay [24, 27]. Thus, both the nature of the curing agent as well as the curing conditions play important roles in the exfoliation process.

Most of the research on epoxy-clay nanocomposites has focused on obtaining either an intercalated or exfoliated structure and studying the influence of these structures on the mechanical properties of the composites, particularly on modulus and strength. Very few studies have investigated the fracture toughness of such nanocomposites and the preliminary results are inconclusive. Using a compact tension specimen, Becker *et al*. [24] found that for a epoxy-nanoclay system containing ammonium ion-modified montmorillanite clay dispersed in bifunctional diglycidyl ether of bisphenol-A (DGEBA) and tetrafunctional tetraglycidyldiamina diphenylmethane (TGDDM) resins, the toughness (and stiffness) increased with clay concentration. On the other hand, Roy *et al*. [29] reported a decrease in fracture toughness with an increase in clay concentration in a bisphenol-A epoxy resin. In the former case, clay particles were dispersed into the epoxy resin using a stirrer at 500 revolutions per minute, whereas in the latter case, clay was hand mixed into the epoxy resin for 20 minutes. The disparity in the two observations is probably due to different clay structures resulting from the different processing techniques used. Therefore, it would be of interest to study the toughening mechanisms in epoxy-clay systems and the influence of clay particles on fracture toughness of these composites as a function of processing parameters and material microstructure, so as to come up with the most suitable processing technique. In the present study, nanocomposites were fabricated with epoxy and clay using two different fabrication processes and investigations are carried out to study their influence on the fracture toughness and flexural modulus of these composites.

2. Material fabrication

The clay used in this study is a commercially available octadecyl ammonium ion modified montmorillonite (MMT) layered silicate (Nanomer® I.30E, Nanocor Inc., Arlington Heights, Illinois, USA) that has a particle size of 8–10 μm. The epoxy resin used is a diglycidyl ether of bisphenol F (Epon 862, Resolution Performance Products, Houston, Texas, USA) which was cured using a moderately reactive, low viscosity aliphatic amine curing agent (Epikure 3274, Resolution Performance Products, Houston, Texas, USA). For mixing the clay with epoxy, a high-speed shear disperser (T-25 ULTRA TURRAX with SV 25 KV–25 F dispersing element, IKA Works Inc., Wilmington, North Carolina, USA) and ultrasonic agitator (750 TSD, Tekmar Co., Cincinnati, Ohio, USA) were used.

A desired amount of clay was added to preheated (60°C) liquid epoxy resin using mechanical mixing. The mixture was mixed for 1 h while maintaining the temperature at 60°C using a hot plate. Subsequently, the mixture was processed with either the high speed shear dispesser (operating at 15,000 rpm) or the ultrasonic agitator (20 kHz frequency; 9.0 sec on-off cycle) for 30 minutes. During this process the temperature of the mixture was maintained at about 65°C by using an ice bath. The mixture was then degassed in a vacuum chamber for 12 h to completely remove trapped air. A stoichiometric amount of

the curing agent was then added and hand mixed gently to avoid introduction of any air bubbles due to mixing action. The final slurry, free of air bubbles, was poured into an aluminum mold and allowed to cure under room temperature for 24 h followed by post curing at 121°C for 6 h. This resulted in a cured sheet of epoxy-clay nanocomposite with the nominal dimensions of 110 × 100 × 6.35 mm. Specimens for fracture toughness and flexural modulus tests were then cut out of this cured sheet. The volume fraction of the clay was varied from 0.5% to 6% to study the influence of clay concentration on mechanical properties. Note that due to difficulties in removing the air bubbles in 6% clay volume nanocomposites processed by ultrasonication, final fabricated plate had minute air bubbles and therefore, experiments were not carried out for this particular case.

3. Measurements

The presence of voids has a deleterious effect on the fracture properties of the composite. Hence, density measurements were performed on all nanocomposites to ensure void free composites. Densities of the plain epoxy and the epoxy-clay nanocomposites were measured using Archimedes' principle as per Equation 1.

$$\rho_s = \frac{\rho_t W_a}{W_a - W_l}, \tag{1}$$

where, ρ_s is the density of specimen, ρ_l is the density of distilled water; W_a and W_l are the weights of specimen in air and distilled water, respectively. At least four samples were tested for each volume fraction and each material process in order to determine the density as per Equation 1.

The flexural moduli of neat epoxy and the epoxy-clay nanocomposites were determined as per ASTM standard D6272–02 [30]. Specimens with a nominal size of 63.5 × 12.7 × 6.35 mm (2.5 × 0.5 × 0.25 in.) were quasi-statically loaded under four-point bending on a bench-top testing frame (Tira Test 2500, TIRA GmbH, Schalkau, Germany) at a crosshead speed of 1.5 mm/minute, with a support span width of 49.6mm and a loading span width of 24.8 mm. The load was measured using a 2000 N load cell, and the load-point specimen displacement was measured using a linear variable displacement transducer (Schaevitz Sensors, Hampton, Virginia, USA). Flexure modulus was studied as a function of volume fraction for the nanocomposites fabricated using the different processes. At least four samples were tested for each volume fraction and each material processing technique used.

Experimental values for flexural modulus were compared with theoretical predictions for Young's modulus using expressions given by Hashin-Shtrikman [31] and Norris [32]. Hashin-Shtrikman bounds for Young's modulus were calculated for a two-phase material using the relation as given in Equation 2,

$$E_x^* = \frac{9K_x^* G_x^*}{3K_x^* + G_x^*}, \tag{2}$$

where, K_x^* represents the estimated bulk modulus and G_x^* represents the estimated shear modulus of the composite, and $x = U$ and $x = L$ for the upper and lower bounds, respectively. The upper and lower bounds on bulk and shear moduli are calculated using Equations 3a–3d [31].

$$K_L^* = K_1 + V_2 \left(\frac{1}{K_2 - K_1} + \frac{3V_1}{3K_1 + 4G_1} \right)^{-1}, \tag{3a}$$

$$K_U^* = K_2 + V_1 \left(\frac{1}{K_1 - K_2} + \frac{3V_2}{3K_2 + 4G_2} \right)^{-1}, \tag{3b}$$

$$G_L^* = G_1 + V_2 \left(\frac{1}{G_2 - G_1} + \frac{6(K_1 + 2G_1)V_1}{5G_1(3K_1 + 4G_1)} \right)^{-1}, \tag{3c}$$

$$G_U^* = G_2 + V_1 \left(\frac{1}{G_1 - G_2} + \frac{6(K_2 + 2G_2)V_2}{5G_2(3K_2 + 4G_2)} \right)^{-1}, \tag{3d}$$

where, K, G and V are the bulk moduli, shear moduli and volume fractions, respectively. The subscript 1 is used for the matrix and subscript 2 for inclusions; $K_2 > K_1$ and $G_2 > G_1$. The bulk and shear moduli of matrix and inclusion were calculated from the Young's modulus and Poisson's ratio using the usual Equations 4a and 4b.

$$K = \frac{E}{3(1 - 2\upsilon)}, \tag{4a}$$

$$G = \frac{E}{2(1 + \upsilon)}. \tag{4b}$$

The Young's modulus, E, and Poisson's ratio, υ, of epoxy were taken as 2.7 GPa and 0.3, respectively. It is common to assign the values of Young's modulus and Poisson's ratio of muscovite for montmorillonite due to the similarities in their crystal structure and chemical composition [33]. Hence, the Young's modulus and Poisson's ratio of clay inclusions were taken as 167 GPa and 0.23, respectively.

A set of expressions, for the prediction of bulk and shear moduli of composites reinforced with inclusions in the form of isotropic oblate spheroids with small aspect ratio and with small volume fractions, were given by Norris [32]. Estimated Young's modulus was also calculated using bulk modulus and shear modulus obtained by using Equations 5a and 5b [32, 33]. In these expressions, the inclusions are considered as homogenously distributed isotropic oblate spheroids with aspect ratio, $\chi = c/a$, where a and c are the equatorial and polar radii, respectively.

$$K = K_1 + \frac{4}{9} V_2 \left[\chi \frac{\pi}{8} \frac{3 - 4\upsilon_1}{G_1(1 - \upsilon_1)} + \frac{1}{G_2} \frac{1 - \upsilon_2}{1 + \upsilon_2} \right]^{-1}, \tag{5a}$$

$$G = G_1 + \frac{1}{15}V_2\left[\chi\frac{\pi}{8}\frac{3-4\upsilon_1}{G_1(1-\upsilon_1)} + \frac{1}{G_2}\frac{1-\upsilon_2}{1+\upsilon_2}\right]^{-1} + \frac{2}{5}V_2\left[\chi\frac{\pi}{16}\frac{7-8\upsilon_1}{G_1(1-\upsilon_1)} + \frac{1}{G_2}\right]^{-1}, \quad (5b)$$

where, K, G and V are the bulk modulus, shear modulus and volume fractions, respectively, as before, and υ is the Poisson's ratio. The subscript 1 is used for matrix and subscript 2 for inclusions. The isotropic spheroid inclusions degenerate into isotropic platelets when the aspect ratio, $\chi = c/a \to 0$.

Fracture tests were carried out on neat epoxy and epoxy-clay nanocomposites using single edge notched specimens having a nominal size of 55.8 × 12.7 × 6.35 mm (2.2 × 0.5 × 0.25 in.). Specimens were quasi-statically loaded under three point bending on the bench-top testing frame. In order to generate a starter crack, first a 4.8 mm deep notch was machined into the specimen using a high-speed diamond saw (MK-370, MK Diamond Products Inc., Torrance, California, USA). Subsequently, a razor blade was inserted into this machined notch and tapped with a small load using a jig designed in-house to generate a small, yet well-controlled starter pre-crack. The peak load, as obtained from the load-displacement curve, was used as the maximum applied force, P, to determine the fracture initiation toughness.

Precise measurement of crack length, a, was done after the fracture experiments using an optical microscope equipped with a micrometer stage. All specimens considered valid for fracture tests have a nominal crack length to specimen width ratio, a/W, of 0.45–0.5, as per ASTM standard 5045 [35]. The fracture initiation toughness was calculated as,

$$K_{Ic} = \frac{P_{\max}}{B\sqrt{W}} f\left(\frac{a}{W}\right), \quad (6)$$

where $P_{\max}$ is the maximum applied force, B is the thickness of specimen, W is width of the specimen and the function f is a geometry factor [36].

In order to investigate the structure of clay formed in the final composites, wide angle X-ray diffraction (WAXD) measurements were carried out on epoxy-clay composites with 0.5 to 6% clay and fabricated by both high shear mixing and ultrasonication using Scintag PAD-X automated diffractometer with a CuK$_\alpha$ radiation ($\lambda = 0.1540$ nm) and a scanning rate of 0.5° per min. The generator was operated at 45 kV and 25 mA. WAXD measurements were also performed on cured samples of neat epoxy (EPON 862) and pure clay powder (Nanocor I.30E). As mentioned earlier, experiments were not performed on 6% clay volume nanocomposites processed by ultrasonication due to difficulties in removing the air bubbles in final fabricated plate.

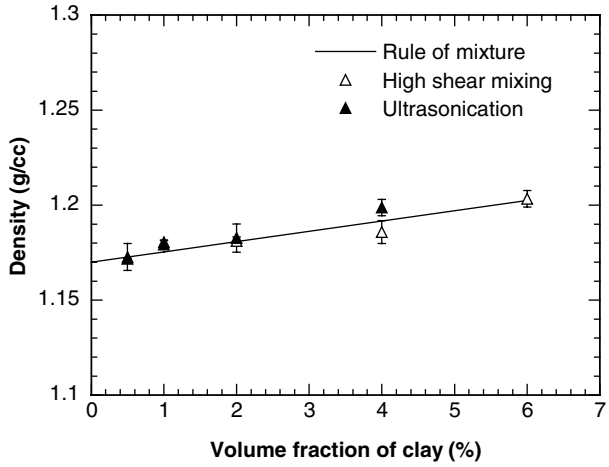

Figure 1 Variation of density as a function of volume fraction of clay for epoxy-clay nanocomposites fabricated using high shear mixing and ultrasonication.

4. Results and discussion

Fig. 1 shows the variation of density with respect to clay volume fraction for epoxy-clay nanocomposites fabricated using high sear mixing and ultrasonication. As expected, the composite density increased directly in proportion with the clay volume fraction. The actual increase in density values was small, for example, the density of neat epoxy (1.17 g/cc) increased by 2% upon the addition of 6% volume fraction of clay. Variations in density are in excellent agreement with calculations based on the rule-of-mixtures approach. Also, no difference in composite density was observed for nanocomposites fabricated using either of the two processing techniques.

Fig. 2 shows the variation of flexural modulus as a function of clay volume fraction for the two types of epoxy-clay nanocomposites along with Hashin-Shtrikman bounds on Young's modulus and theoretical estimates of Young's modulus calculated using Equations 5a and 5b

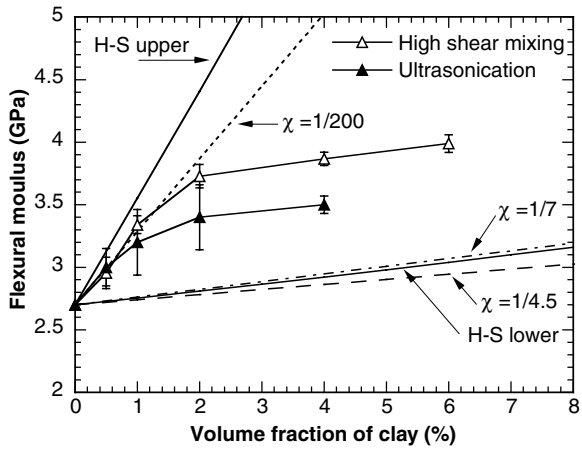

Figure 2 Variation of flexural modulus as a function of clay volume fraction for nanocomposites fabricated by high shear mixing and ultrasonication along with theoretical predictions using expressions given by Hashin-Shtrikman [31] and Norris [32].

[32, 33] and with different aspect ratios, χ. In general, the modulus increased monotonically with the addition of clay. However, the rate of increase was greater at lower volume fractions. Also, while the trends were similar, the absolute values of modulus were higher for nanocomposites fabricated using high shear mixing as compared to those using ultrasonication. The overall increase in modulus was significant, especially for materials processed using high-shear, for example at a clay volume fraction of 6% the nanocomposite modulus was 35% higher than that for nanocomposites containing 0.5% clay by volume, for the nanocomposites fabricated by shear mixing. These improvements in properties are significant considering the increase in weight of the nanocomposites, which is merely 2%. Earlier, it was shown by Lan and Pinnavaia [26] that there is a significant improvement in the tensile modulus with increased clay volume fractions and exfoliation of clay in epoxy-clay nanocomposites. It is seen that, at lower volume fractions (0 to 2%), the experimental values lie close to theoretical prediction of modulus based upon completely exfoliated and homogenously distributed platelets with aspect ratio $\chi = 1/200$. This is true for both composites prepared by both shear mixing and ultrasonication. For clay volume fractions greater than 2%, the composites fabricated by high shear mixing and ultrasonication behave like two-phase composites with spheroids having aspect ratio $\chi = 1/7$ and $\chi = 1/4.5$, respectively. In the light of X-ray diffraction observations, which, as discussed later, point towards complete exfoliation even at the higher clay loadings, the decreasing rate of modulus improvement may be attributed to the presence of isolated clay aggregates at higher volume fractions. A similar trend for modulus has been reported previously in literature [37]

Fig. 3 shows the variation of fracture toughness as a function of clay volume fraction for the nanocomposites fabricated by high speed shear mixing and ultrasonication. In the case of epoxy-clay nanocomposites fabricated using shear mixing, the fracture toughness increased by about 35%, as compared to that of neat epoxy, for a clay volume fraction of 2%. As the clay loading was increased further, the fracture toughness remained constant till a clay volume fraction of 4%. However, the fracture toughness started to decrease beyond this point as the clay volume fraction was increased even further to 6%. Similarly, the nanocomposites fabricated using ultrasonication showed an increase of about 20% in the fracture toughness at a clay volume fraction of 2% and dropped slightly for a clay volume fraction of 4%. Experiments were not conducted on nanocomposites fabricated using the ultrasonication with 6% clay volume fraction because of the presence of air bubbles in the fabricated material. At low volume fractions of clay ($< 1\%$), epoxy-clay nanocomposites prepared by ultrasonication exhibited greater increase in toughness compared to those prepared by shear mixing. Beyond this point ($\geq 1\%$), nanocomposite samples fabricated using shear mixing show greater increase (about 13% higher) in toughness. The improvements in the mechanical properties of epoxy-clay nanocomposites over neat epoxy can be attributed to the dispersion of clay and the exfoliation of clay particles, which is indicated by

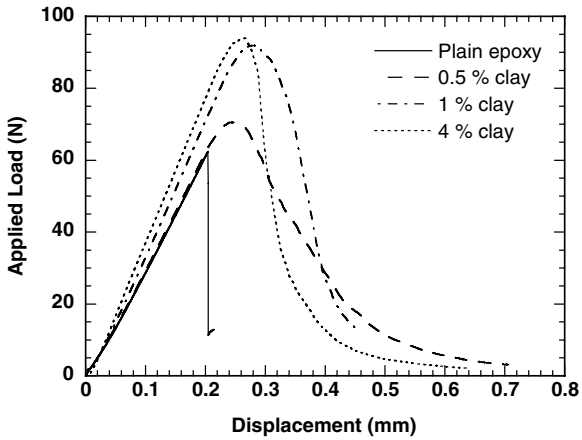

Figure 4 Plots of applied load against cross-head displacement for plain epoxy specimen and nanocomposite specimens fabricated using high shear mixing obtained during fracture experiments.

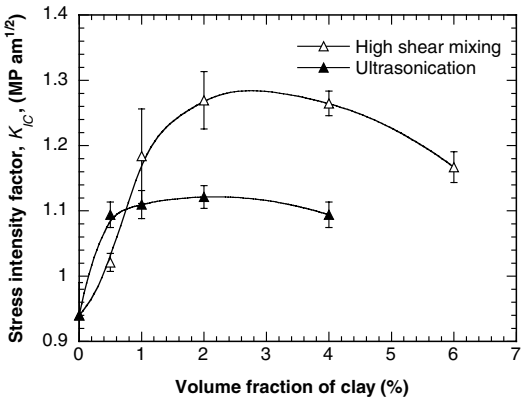

Figure 3 Variation of stress intensity factor as a function of volume fraction of clay for epoxy-clay nanocomposites fabricated using high shear mixing and ultrasonication.

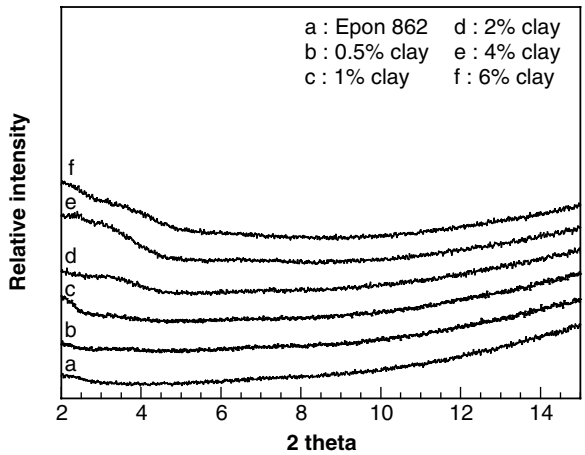

Figure 5 WAXD patterns for epoxy-clay composites with varying clay loadings fabricated using high shear mixing.

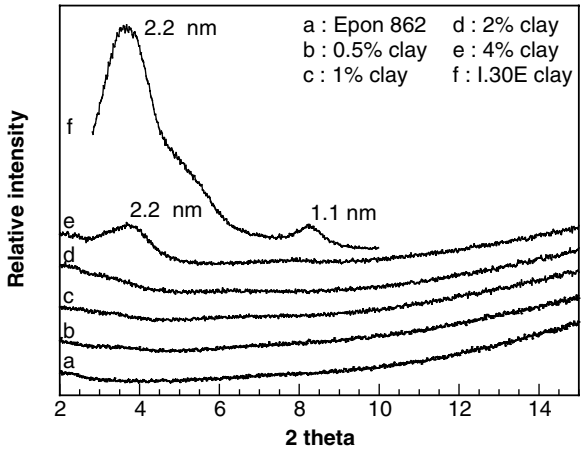

Figure 6 WAXD patterns for epoxy-clay composites with varying clay loadings fabricated using ultrasonic mixing.

XRD measurements as discussed later. Although the XRD measurements suggest complete exfoliation of clay even for higher volume fractions of clay in case of epoxy-clay composites prepared by high shear mixing, isolated particle agglomerates could leads to reduced fracture toughness in these composites. These particle agglomerates can act as failure sites from where the crack initiates and thus influence the values of the critical stress intensity factor, K_{Ic}.

Fig. 4 shows the load-displacement plots obtained during the fracture experiments conducted on single edged notched specimens of epoxy-clay nanocomposites prepared by high shear mixing along with one that corresponds to plain epoxy. All the plots are from specimens with similar initial pre-crack length to aid in direct comparison. The nature of the fracture process can be inferred from these load-displacement plots. Neat epoxy exhibits

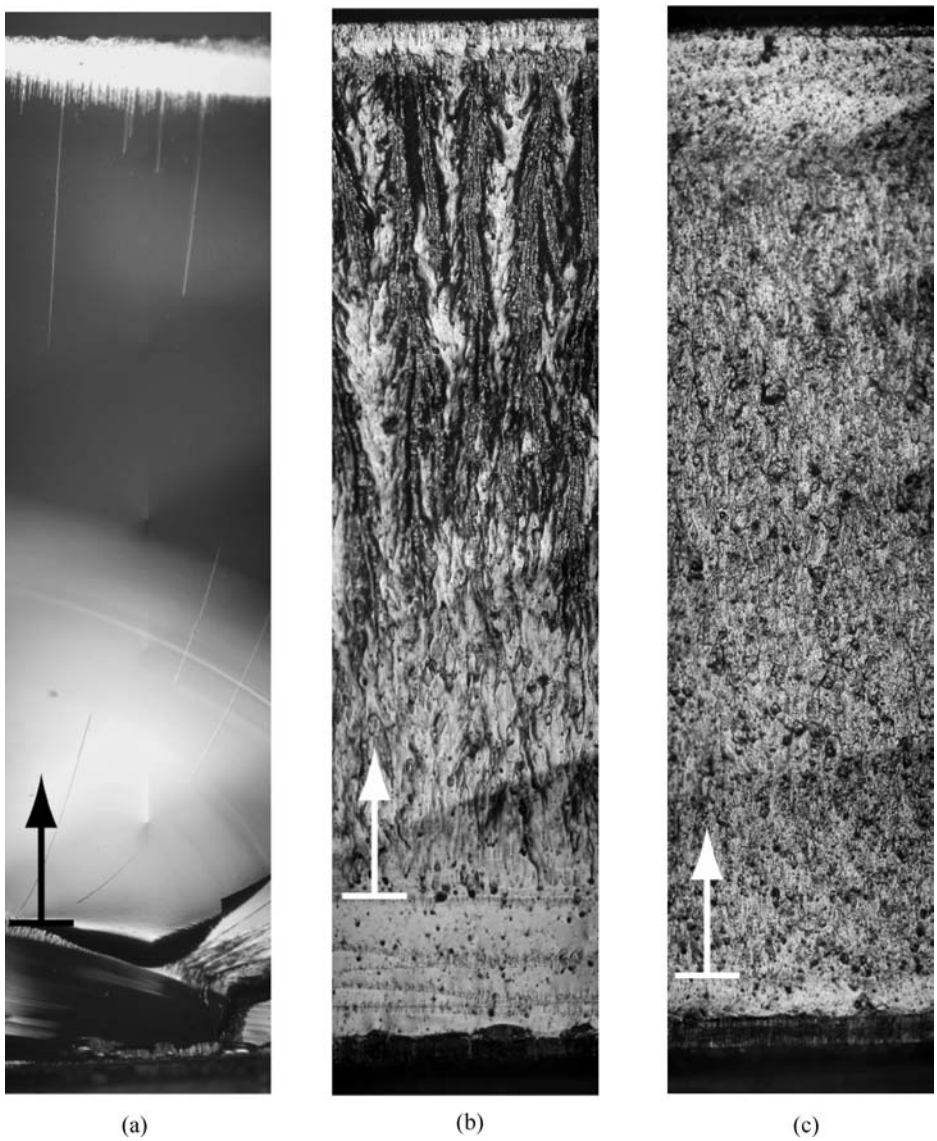

Figure 7 Optical micrographs showing fracture surfaces of specimens subjected to 3 point bending fracture experiments for (a) neat epoxy, (b) nanocomposites fabricated by high shear mixing with 0.5% clay volume fraction, and (c) nanocomposites fabricated by high shear mixing with 2% clay volume fraction. The arrow denotes the location where the crack initiated under loading and also the direction of crack propagation.

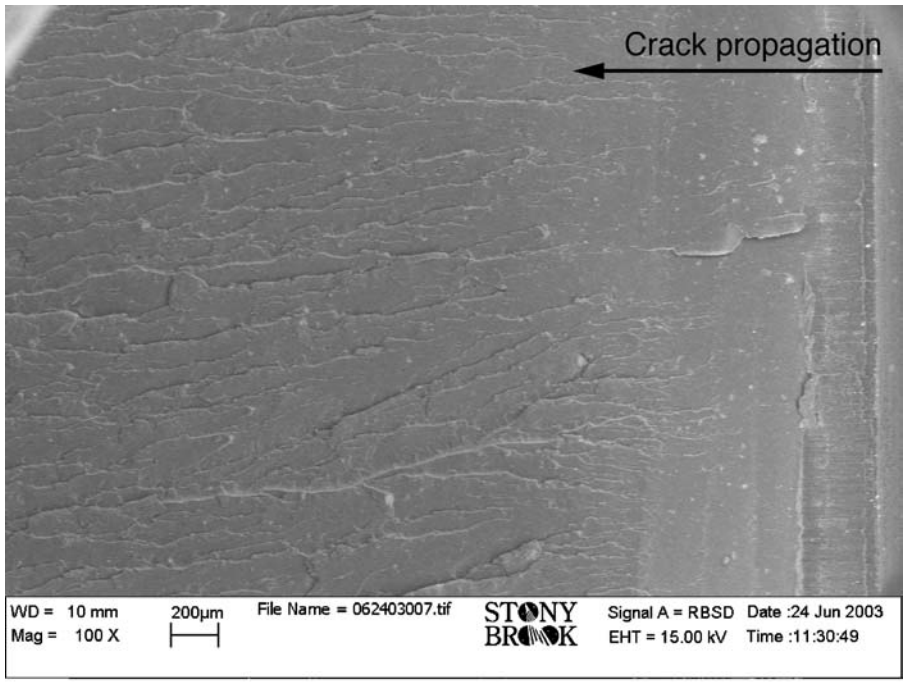

(a)

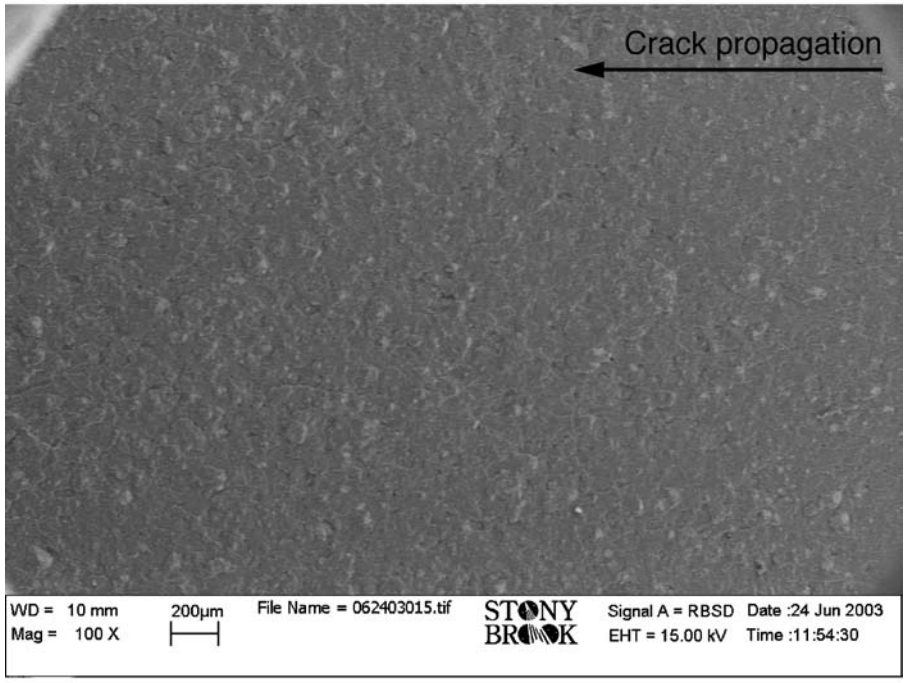

(b)

Figure 8 SEM micrographs of fracture surface of epoxy-clay nanocomposites fabricated by high shear mixing (a) 1% clay volume fraction, (b) 6% clay volume fraction.

brittle fracture as the plot shows a sudden drop in load upon attainment of the peak load corresponding to fracture initiation. On the other hand, the plots obtained for nanocomposite specimens show a gradual decrease in the load after attainment of the peak load, which shows that there is sub-critical crack growth and that toughening is taking place in these nanocomposites.

For materials that do not exhibit crack growth related toughening, the failure is expected to be catastrophic, as observed for neat epoxy. In contrast, the failure behavior of the nanocomposites shows that considerable increase in fracture toughness (crack growth resistance) occurs with the increasing crack length, even at very small volume fractions of clay. The load-displacement plots shown in

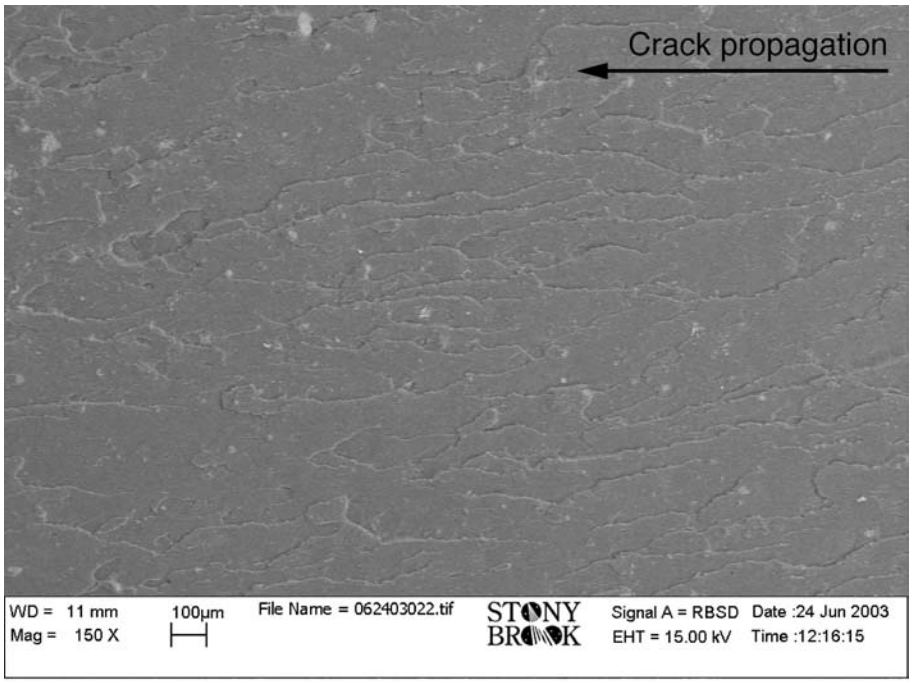

(a)

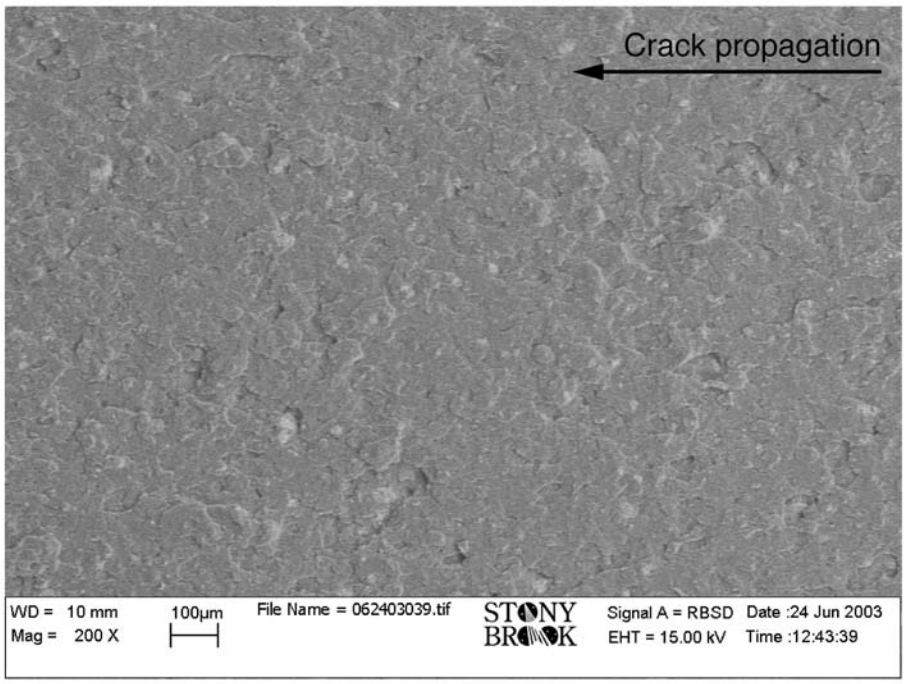

(b)

Figure 9 SEM micrographs of fracture surface of epoxy-clay nanocomposites fabricated by ultrasonication (a) 1% clay volume fraction, (b) 6% clay volume fraction.

Fig. 4 also confirm the increase in modulus with the increase in clay volume fraction.

XRD analyses were performed on epoxy-clay specimens prepared by using high shear mixing and ultrasonication. Figs 5 and 6 show the diffractograms obtained for epoxy-clay specimens prepared by using high shear mixing with clay volume fraction of 0 to 6% (Fig. 5a to 5f) and ultrasonication with clay volume fraction of 0 to 4% (Fig. 6a to 6e), respectively. No prominent peak is seen in the diffractograms of any of the samples fabricated using high shear mixer (Fig. 5). This indicates that complete exfoliation is achieved for these samples. The only epoxy-clay composite showing a distinct peak is the one with 4% clay and fabricated using ultrasonication (6e).

It shows a characteristic peak at 2.2 nm corresponding to the (001) plane. Relative intensity obtained for pure I.30E clay powder is also shown (6f) in which characteristic peaks corresponding to (001) and (002) planes can be seen at 2.2 nm and 1.1 nm, respectively. From Fig. 6, it can be inferred that an exfoliated clay structure is obtained for clay loadings of 0.5 to 2%, whereas the clay structure is unaltered for 4% clay loading.

Morphologies of fractured surfaces of nanocomposite specimens that were tested for fracture toughness were studied under an optical microscope and also using scanning electron microscopy (SEM). Fig. 7 shows the optical micrographs of the fracture surface across the specimen for neat epoxy (7a), and epoxy fabricated using the high shear mixer with 0.5% clay (7b) and 2% clay (7c). Figs 8 and 9 show SEM micrographs of the fracture surface of epoxy-clay nanocomposites processed using high-shear mixing and ultrasonication, respectively, for clay volume fractions of 1% and 6%. Differences in scattering densities of clay and epoxy facilitate differentiation of clay aggregates, and hence, their characteristics and distribution. These micrographs provide important insights regarding clay distribution, particle-crack interaction, and particle-matrix interface, and help in better understanding the processing-structure-property relationships. The fracture surfaces of neat epoxy specimens exhibited a clean featureless surface that results from brittle failure of epoxy. In contrast, fracture surfaces of all the epoxy-clay nanocomposites show greatly increased roughness characterized by 'river-line' markings. These marking indicate the presence of extrinsic toughening mechanisms such as crack path deflection and micro-cracking which result in increased resistance to crack propagation in the clay reinforced nanocomposites. Also, as can be seen for Figs 7, 8 and 9, the river-line markings were more prominent for specimens containing lower volume fractions of clay (0.5% and 1% clay). This was true for the composites processed using both the techniques: high shear mixing and ultrasonication. Fewer river markings were observed in fracture specimens with higher clay loadings that also exhibited large particle agglomerates and reduced fracture toughness. Both the high shear mixing and ultrasonication techniques were capable of breaking particle agglomerates in nanocomposites to some extent for clay volume fractions under 2%. However, at higher clay volume fractions, isolated particle agglomerates were present in nanocomposites fabricated using both the techniques.

5. Conclusion

Influence of processing parameters and particle volume fraction on the mechanical properties of epoxy-clay nanocomposites was studied. Nanocomposites were fabricated using two different processing techniques viz., high speed shear mixing and ultrasonication, and clay volume fraction was systematically varied from 0.5 to 6%. Flexural modulus and fracture toughness of the nanocomposites were measured and fracture surfaces were characterized using scanning electron microscopy. It was observed that addition of clay particles in epoxy resulted in considerable toughening of the nanocomposites leading to slow crack growth. Of the two processing techniques investigated, high speed shear mixing resulted in better dispersion of clay particles and better mechanical properties than ultrasonication. In both the cases, flexural modulus increased monotonously with clay volume fraction, whereas fracture toughness values exhibited an initial increase, and then a drop following a brief plateau region. Experimental values of flexural modulus lie within Hashin-Shtrikman bounds calculated for a two-phase composite. Also, comparison with theoretical predictions suggests that, at lower clay volume fractions, the composites fabricated by both high shear mixing and ultrasonication behave as nanocomposites with homogenously dispersed exfoliated platelets. X-ray diffraction studies confirm the exfoliated clay structure in all the composites except one with 4% clay volume fraction and mixed using ultrasonication. The drop in fracture toughness is attributed to the presence of isolated particle agglomerates at higher clay volume fractions as was evident from the SEM micrographs. Particle agglomerates, and their detrimental effect on the mechanical properties of the nanocomposites were seen at much higher clay volume fraction of 6% in the nanocomposites fabricated by shear mixing as compared those prepared by ultrasonication where these effects were observed at a relatively lower clay volume fraction of 4%. This shows that, of the two fabrication techniques studied, high shear mixing leads to better dispersion and hence superior mechanical properties in the epoxy-clay nanocomposites, albeit with a limitation on volume fraction.

Acknowledgements

The authors gratefully acknowledge the support of the National Science Foundation via Grant No. CMS 0099629.

References

1. R. A. VAIA and E. P. GIANNELIS, *MRS Bull.* **26** (2001) 394.
2. X. KORNMANN, L. A. BERGLUND, J. STERTE and E. P. GIANNELIS, *Polym. Eng. Sci.* **38** (1998) 1351.
3. E. P. GIANNELIS, *Adv. Mater.* **8** (1996) 29.
4. R. P. SINGH, M. ZHANG and D. CHAN, *J. Mater. Sci.* **37** (2002) 781.
5. S. C. ZUNJARRAO and R. P. SINGH, in Proceedings of the 2004 SEM X International Congress & Exposition on Experimental and Applied Mechanics, Costa Mesa, California USA, (Society for Experimental Mechanics, Inc., 2004) p. 375.
6. C. B. NG, L. S. SCHADLER and R. W. SIEGEL, *Nanostruct. Mater.* **12** (1999) 507.
7. A. ALLAOUI, S. BAI, H. M. CHENG and J. B. BAI, *Compos. Sci. Technol.* **62** (2002) 1993.
8. R. KRISHNAMOORTI and R. A. VAIA, in Proceedings of the 219th National Meeting of the American Chemical Society, Mar 26-30 2000, San Francisco, CA, United States, edited by R. A. Vaia (Oxford University Press, 2002) p. 225.
9. T. J. PINNAVAIA, T. LAN, Z. WANG, H. Z. SHI and P. D. KAVIRATNA, "Nanotechnology" (American Chemical Society, 1155 Sixteenth St NW, Washington, DC 20036, 1996).

10. Y. KOJIMA, A. USUKI, M. KAWASUMI, A. OKADA, Y. FUKUSHIMA, T. KURAUCHI and O. KAMIGAITO, *J. Mater. Res.* **8** (1993) 1185.
11. A. USUKI, Y. KOJIMA, M. KAWASUMI, A. OKADA, T. KURAUCHI and O. KAMIGAITO, in Proceedings of the Washington, *DC Meeting* **1990** of the ACS, Division of Polymer Chemistry, Aug 26-31 1990, Washington, DC, USA, (ACS, Washington, DC, USA, 1990) p. 651.
12. T. M. WU and J. Y. WU, J. *Macromol. Sci., Phys.* **41 B** (2002) 17.
13. K. MASENELLI-VARLOT, E. REYNAUD, G. VIGIER and J. VARLET, *J. Polym. Sci., Part B: Polym. Phys.* **40** (2002) 272.
14. T. J. PINNAVAIA, T. LAN, P. D. KAVIRATNA and M. S. WANG, in Proceedings of the 1994 MRS Spring Meeting, Apr 4-8, 1994, San Francisco, CA, USA, (Materials Research Society, Pittsburgh, PA, USA, 1994) p. 81.
15. T. AGAG, T. KOGA and T. TAKEICHI, *Polymer* **42** (2001) 3399.
16. M. O. ABDALLA, D. DEAN and S. CAMPBELL, in Proceedings of the Organic/Inorganic Hybrid Materials 2002, Apr 1-5 2002, San Francisco, CA, United States, (Materials Research Society, 2002) p. 179.
17. M. MEHRABZADEH, M. R. KAMAL and V. MOLLET, in Proceedings of the 61st Annual Technical Conference ANTEC 2003, May 4-8, 2003, Nashville, TN, United States, (Society of Plastics Engineers, 2003) p. 2260.
18. F. D. KUCHTA, P. J. LEMSTRA, A. KELLER, L. F. BATENBURG and H. R. FISCHER, in Proceedings of the Materials Research Society Symposium - 1999 MRS Spring Meeting - Symposium DD, 'Organic/Inorganic Hybrid Materials', Apr 5-Apr 9, 1999, San Francisco, CA, USA, (Materials Research Society, Warrendale, PA, USA, 1999) p. 363.
19. G. CHEN, X. CHEN, Z. LIN and W. YE, *J. Mater. Sci. Lett.* **18** (1999) 1761.
20. G. J. JIANG and H. Y. TSAI, *American Chemical Society, Polymer Preprints, Division of Polymer Chemistry, The San Francisco Meeting, Mar 26-Mar 31, 2000* **41** (2000) 621.
21. M. PRAMANIK, B. K. SAMANTARAY, A. K. BHOWMICK and S. K. SRIVASTAVA, *J. Polym. Sci., Part B: Polym. Phys.* **40** (2002) 2065.
22. Y. TANG, Y. HU, J. WANG, R. ZONG, Z. GUI, Z. CHEN, Y. ZHUANG and W. FAN, *J. Appl. Polym. Sci.* **91** (2004) 2416.
23. M. ALEXANDRE and P. DUBOIS, *Mater. Sci. Eng., R* **28** (2000) 1.
24. O. BECKER, R. VARLEY and G. SIMON, *Polymer* **43** (2002) 4365.
25. D. RATNA, N. R. MANOJ, R. VARLEY, R. K. S. RAMAN and G. P. SIMON, *Polym. Int.* **52** (2003) 1403.
26. T. LAN and T. J. PINNAVAIA, *Chem. Mater.* **6** (1994) 2216.
27. X. KORNMANN, H. LINDBERG and L. A. BERGLUND, *Polymer* **42** (2001) 4493.
28. *Idem.*, *ibid.* **42** (2001) 1303.
29. S. ROY, H. LU, S. PERIASAMY and J. MA, in Proceedings of the 44th AIAA/ASME/ASCE/AHS/ASC Structures, Structural Dynamics, and Materials Conference, Norfolk, VA, United States, (American Inst. Aeronautics and Astronautics Inc., 2003) p. 2761.
30. AMERICAN SOCIETY OF TESTING AND MATERIALS, "Standard Test Method for Flexural Properties of Unreinforced and Reinforced Plastics and Electrical Insulating Materials by Four-Point Bending", Annual Book of ASTM standards, Designation: D6272-02, 2003.
31. Z. HASHIN and S. SHTRIKMAN, *J. Mech. Phys. Solids* **11** (1963) 127.
32. A. N. NORRIS, *Int. J. Solids Struct.* **26** (1990) 663.
33. J. WANG and R. PYRZ, *Compo. Sci. Tech.* **64** (2004) 925.
34. *Idem.*, *ibid.* **64** (2004) 935.
35. AMERICAN SOCIETY OF TESTING AND MATERIALS, "Standard Test Methods for Plane-Strain Fracture Toughness and Strain Energy Release Rate of Plastic Materials", Annual Book of ASTM Standards, Designation: D5045-99, 1999.
36. T. L. ANDERSON, "Fracture Mechanics: Fundamentals and Applications" (CRC Press, Boca Raton, FL, 1991).
37. A. YASMIN, J.L. ABOT, and I.M. DANIEL, *Scripta Materialia* **49** (2003) 81.

Received 2 May
and accepted 6 July 2005